RSC Advances

PAPER

View Article Online
View Journal | View Issue

Cite this: *RSC Adv.*, 2026, **16**, 24916

Design and optimization of a Cu-MOF@graphene oxide nanozyme for point-of-care colorimetric determination of sarcosine and H_2O_2

Martin N. Saad, *[a] Amr M. Mahmoud, [a] Sawsan M. Amer, [a] Ibrahim M. El-Sherbiny *[b] and Hoda M. Marzouk [a]

Prostate cancer is a leading cause of tumor-related mortality worldwide, and there is a critical need for reliable biomarkers that enable early, accurate, and specific diagnosis. Sarcosine, a metabolic byproduct of glycine, has emerged as a potential biomarker for prostate cancer progression, but its low physiological concentration and interference from complex biological matrices make its detection analytically challenging. In this study, a copper-based metal–organic framework supported on graphene oxide (Cu-MOF@GO) was synthesized *via* a solvothermal method and used as a highly active peroxidase-like nanozyme for the colorimetric detection of hydrogen peroxide and sarcosine. The Cu-MOF was successfully anchored onto the graphene oxide surface, providing an exceptionally large surface area (1476.8 m^2 g^{-1}) and abundant catalytic sites, as confirmed by structural and surface characterization through FTIR, SEM-EDX, BET and XRD analyses. To optimize catalytic efficiency, a half-fractional Central Composite Design (CCD) was employed, leading to excellent correlation coefficients (R^2 > 0.999) for linear responses to hydrogen peroxide (0.5–1000 μM, with a detection limit of 0.15 μM) and sarcosine (0.5–250 μM, with a detection limit of 0.16 μM). The method also demonstrated strong potential for portable analysis using smartphone-based RGB color detection, showing high precision and recovery in spiked serum samples. This work presents a computationally guided approach for designing nanozymes with enhanced catalytic activity, offering a low-cost, rapid sensor with wide linearity, high sensitivity, and unique selectivity for sarcosine detection, making it promising for portable and point-of-care prostate cancer screening applications.

Received 24th February 2026
Accepted 2nd May 2026

DOI: 10.1039/d6ra01609j

rsc.li/rsc-advances

1. Introduction

Prostate cancer is a key global health crisis, with more than 1.3 million new cases being diagnosed every year. It remains the most commonly occurring malignancy among men and categorized as the second leading cause of cancer-related death globally.[1] That is why there is a need for a specific, sensitive and accurate method that can help with early diagnosis and prevent millions of casualties. The prostate-specific antigen (PSA) screening test was developed for this reason. However, many patients got false positive or negative results upon analysis of PSA.[2,3] Among the metabolic biomarkers being studied in relation to prostate cancer, sarcosine (Sar) $C_3H_7NO_2$ has gained much attention for its involvement in tumor growth and metastasis. Sarcosine is a naturally occurring, non-proteinogenic amino acid produced by glycine and is also a metabolite of choline, predominantly located in the skeletal muscle and prostate tissue.[4,5] In healthy individuals, serum sarcosine levels are generally approximately 1.4 ± 0.6 μM and 2–10 μM in prostate cancer patients.[6–8] High levels of sarcosine have been associated with the initiation and progression of prostate cancer, and its determination in biological samples such as tissue, urine, or plasma has been suggested as a promising biomarker for disease diagnosis and monitoring. Challenges facing determination of sarcosine are the trace level concentration in healthy individuals and the interferences presented by the biological matrices and other amino acids.[9] For those reasons, a specific and highly sensitive method would offer a perfect solution for the analysis of such important biomarker.

Numerous approaches have been reported in literature for the determination of sarcosine including chromatographic methods,[10,11] spectro–fluorimetric methods,[12–14] capillary electrophoresis,[15] electrochemical methods,[16,17] among others. The chromatographic methods are excellent in separation but need expensive equipment, solvents and operator skills. The fluorimetric method is sensitive but, in most cases, needs

[a]*Pharmaceutical Analytical Chemistry Department, Faculty of Pharmacy, Cairo University, El-Kasr El-Aini Street, 11562 Cairo, Egypt. E-mail: martin.nady@pharma.cu.edu.eg*

[b]*Nanomedicine Research Labs, Center for Materials Science CMS, Zewail City of Science and Technology, 6th October City, 12578, Giza, Egypt. E-mail: ielsherbiny@zewailcity.edu.eg*

derivatization, extensive sample preparation to remove interferences and also costly equipment. The electrochemical methods have the advantages of no sample preparation but suffer from low sensitivity and selectivity. Colorimetric methods offer simple, cheap, direct and easy to apply methods that have been known for decades. Various colorimetric methods have been reported for determination of sarcosine and H_2O_2.[14,18–29] However, those methods show narrow linearity range, low sensitivity and selectivity. There is still a gap that needs to be filled with simple, easy, cost effective, specific and highly sensitive method for the analysis of sarcosine that could solve problems of early diagnosis difficulty for prostate cancer.

Natural enzymes have excellent catalytic efficiency and can be widely used in various colorimetric assays under mild conditions; however, their practical applications are significantly restricted by intrinsic instability, high cost, and sensitivity to environmental factors.[30,31] In order to overcome these challenges, recent efforts have been directed toward the development of advanced catalysts and functional materials with enzymatic activities that propose more sensitive, stable, and economical substitute to traditional enzyme-based sensors.[32] Nanomaterials have numerous applications due to their unique surface area to volume ratio.[33–43] Correspondingly, metal nanostructures and carbon-dependent nanomaterials (in particular, MOFs) have recently emerged as highly versatile candidates due to their unique physicochemical properties combined with tunable structures.[37,44–50] In MOFs, enzyme-like catalytic behavior originates from redox-active metal centers coordinated with organic ligands, which greatly facilitate efficient electron transfer during the course of the reactions.[51–55] MOFs (Metal–Organic Frameworks) mimic enzymes due to their structural and catalytic properties. They possess a porous structure, offering high surface area for catalysis, with metal centers acting as active sites, similar to enzyme active sites. MOFs are selective for certain substrates based on their pore size and metal centers, akin to the specificity enzymes have for substrates.[56] MOFs can accelerate chemical reactions like enzymes, including oxidation, hydrolysis, and reduction, with their metal ions functioning as Lewis acids, similar to metalloenzymes. The metal centers facilitate reactions typically associated with biological systems. Additionally, multiple catalytic mechanisms, such as hydrogen bonding, electron transfer, and substrate binding, allow MOFs to mimic enzyme-like behaviors and catalyze reactions with high efficiency.[57] Among various MOFs, Cu-based systems have shown remarkable peroxidase-like activity.[19,58–60] The uniformly distributed active sites within MOF structures allow intimate substrate interaction during catalysis, resulting in outstanding catalytic performance and efficient H_2O_2 reduction through biomimetic redox processes.[31] Graphene oxide is a material that is strong, flexible, and hydrophilic, with high surface area and moderate electrical conductivity.[61] Combining Cu-MOF with graphene oxide would help increase the surface area and porosity and also increase the short term as well as long term stability.

The proposed work introduces a novel Cu-MOF@ graphene oxide (GO) nanozyme designed specifically for the colorimetric quantification of both hydrogen peroxide (H_2O_2) and the prostate cancer biomarker sarcosine. The analytical detection of sarcosine follows a highly specific, two-stage enzymatic and biomimetic cascade. In the initial recognition phase, the natural enzyme sarcosine oxidase (SOX) catalyzes the oxidative demethylation of sarcosine into glycine and formaldehyde.[62] A critical byproduct of this enzymatic reaction is the stoichiometric generation of hydrogen peroxide H_2O_2, the concentration of which is directly proportional to the initial amount of sarcosine present. In the subsequent signaling phase, the synthesized Cu-MOF@GO nanozyme functions as a high-efficiency peroxidase-mimicking nanozyme. Utilizing its abundant Cu^{2+} active sites anchored on the high-surface-area graphene oxide support, the nanozyme facilitates a reaction that decomposes the generated H_2O_2 into highly reactive hydroxyl radicals ($OH^{\cdot}$).[29] These radicals immediately drive the oxidation of the chromogenic substrate, *o*-phenylenediamine (OPD), from a colorless state to the yellow-colored product 2,3-diaminophenazine (DAP).[19] The intensity of this yellow color, quantitatively assessed *via* its maximum absorbance at 450 nm, serves as the analytical signal for the ultrasensitive determination of sarcosine, enabling a seamless transition from a metabolic biomarker to a measurable optical output.[18]

In this study, a copper-based MOF was uniformly anchored onto the surface of graphene oxide through a solvothermal assembly method, forming a highly stable composite with a large surface area and abundant accessible active sites. The incorporation of GO enhanced electron transport and catalytic efficiency, leading to superior peroxidase-like activity compared with polymer-supported analogues. Unlike inert polymers, GO provides oxygen-containing functional groups (carboxyl, hydroxyl) that act as coordination sites for the Cu^{2+} nodes, ensuring high dispersion and preventing leaching.[63] Furthermore, the conjugated structure of GO facilitates faster electron transfer during the redox cycle of H_2O_2, which is the rate-limiting step in peroxidase-like catalysis.[64] Additionally, the high aspect ratio and sheet-like structure of GO allow for better dispersion of Cu-MOF crystals and more efficient interaction with analytes, thereby enhancing the catalytic performance of the nanozyme.[65,66] The material was thoroughly characterized by FTIR, SEM-EDX, BET and XRD analyses, confirming homogeneous distribution and intimate interaction between the Cu-MOF framework and the GO matrix. The Cu-MOF@GO nanozyme was optimized *via* a half-fractional central composite design (CCD) to achieve maximum catalytic performance toward OPD oxidation in the presence of H_2O_2. The method has been applied for determination of sarcosine in serum samples. The sensor has been integrated into Arduino based portable device that can allow online monitoring. The developed platform provides a sensitive, selective and cost-effective colorimetric assay for both H_2O_2 and sarcosine, with capacity to apply in point-of-care settings for prostate cancer screening. The method provides exceptionally wide linearity range and lower detection limits than previously reported methods. This work represents a significant advancement in nanozyme-based biosensing systems, driven by Four key factors. First, catalytic enhancement is achieved through the integration of Cu and GO in the prepared nanozyme. The second factor is statistical

optimization *via* the Central Composite Design (CCD) experimental approach, and the third factor is the biomarker specificity, as shown by the selectivity study. The fourth factor is the application of the proposed sensor using the Arduino based portable device to allow point of care biomarker quantification.

2. Material and methods

2.1. Instruments

Spectrophotometric measurements were performed using the UV probe version 2.21 program and Shimadzu double beam UV-visible spectrophotometer (model: 1610, Tokyo, Japan). Fourier transform infrared spectroscope (FTIR) analysis of samples was conducted on a Nicolet 380 FTIR using the KBr disk technique. Resolution is 4 and 16 scans were accumulated for each spectrum in a range of 500–4000 cm^{-1}. Brunauer–Emmett–Teller (BET) measurements (Quanta chrome Touch Win™ version 1.2) were applied to determine the surface area and porosity of the nanozymes. SEM measurements were done using Quanta FEG250 electron microscope, Thermo Fischer Scientific (FEI), S15A sputter coater with EDX (energy dispersive X-ray analysis). Teflon lined hydrothermal autoclave was used for the Cu MOF preparation.

2.2. Materials and reagents

The investigation used high analytical grade solvents and double-distilled deionized water from the Milli-Q equipment (Millipore Corporation, France). Sigma Aldrich (Steinheim, Germany) provided *N*,*N*-dimethylformamide anhydrous (DMF), copper sulfate, graphene oxide (GO), benzene-1,3,5-tricarboxylate (BTC or trimesic acid), methanol, hydrogen peroxide, *o*-phenylenediamine (OPD), sarcosine oxidase (SOX), and sarcosine (Sar or *N*-methyl glycine). PioChem (Cairo, Egypt) provided sodium hydroxide pellets, hydrochloric acid, glacial acetic acid, sodium acetate, potassium dihydrogen phosphate, and dipotassium hydrogen phosphate. All the cited chemicals are of analytical grade with purity (95% to 99%). Samples of human serum and urine were collected with permission from the Holding Company of Biological Products and Vaccines, VACSERA (Giza, Egypt).

2.3. Preparation of Cu MOF@GO nanozyme

Solvothermal technique was utilized[67] wherein 50 g of GO was put into a falcon tube, ultrasonically disseminated for 20 min in 20 ml DMF, and then 478 mg of $CuSO_4$ was added and then magnetically agitated for fifteen min. at room temperature. In the meantime, 10 ml of DMF was used to dissolve 420 milligrams of trimesic acid in another beaker. After transferring the second beaker to the first, they were moved to a hydrothermal oven and baked for 12 h. at 140 °C. The resulting MOF powder was then recovered by centrifugation, cleaned with DMF, water, and methanol, three times for each solvent and dried for two h at 60 °C in a vacuum drying oven. The produced nanozymes were collected in Eppendorf tube and stored at 4 °C in the refrigerator till use. In this approach, the metal precursor and organic linker are dissolved in a suitable solvent, sealed, and heated for a defined duration to promote controlled crystal nucleation and growth. The precisely maintained reaction environment allows fine control over crystal morphology and particle uniformity. In this work, copper was chosen as the central metal due to its excellent catalytic properties, structural flexibility, high thermal and chemical stability, intrinsic porosity, and low cost. Trimesic acid (BTC) was the organic linker; its three symmetrically positioned carboxylate groups on the benzene ring coordinate effectively with Cu^{2+} ions at multiple angles, constructing a robust and highly porous framework with a large surface area and stability. Anhydrous *N*,*N*-dimethylformamide (DMF) was used as the reaction medium because of its good solubility for both metal salts and organic ligands, which facilitates the formation of well-defined MOF crystals. Graphene oxide (GO) was introduced as a supporting matrix to further enhance dispersion and electron transfer, while increasing the surface area for anchoring Cu-MOF. Such a hybrid structure favored the accessibility of catalytic sites and greatly enhanced the peroxidase-like activity of the nanozyme, enabling highly sensitive colorimetric detection for H_2O_2 and sarcosine.

2.4. Cu MOF@GO peroxidase like activity and detection of H_2O_2 using colorimetry

In order to check the peroxidase mimetic activity of the prepared nanozymes, OPD was utilized. Peroxidase enzyme can oxidize OPD (colourless solution) in presence of H_2O_2 to produce diamino-phenazine DAP (yellow solution). The reaction starts with the H_2O_2 being decomposed at the metal centers of the nanozymes, forming reactive oxygen species (ROS), which further oxidize the OPD substrate to a product known as 2,3-diaminophenazine or (DAP). The DAP produced is visually detectable due to its yellow colour which correlates to the concentration of H_2O_2, Fig. S1. Test was done by adding 360 μL of 10 mM OPD to 360 μL of 10 mM H_2O_2 and 10 μL of Cu-MOF@GO nanozyme (1 mg ml^{-1}) all prepared using double distilled water. The previous mixture was added to 2770 μL 0.1 M acetate buffer pH 4.0. The acetate buffer was prepared as per European pharmacopeia.[68] The pH is one of the main factors affecting the performance of the nanozyme peroxidase activity, so acetate buffer was prepared in order to control the pH. The resulting solution was put for 10 min into a 40 °C water bath. The reaction was then assessed by measuring the absorbance of the oxidized OPD at 450 nm and recording the solution's UV-vis spectra throughout the range 300–600 nm. Afterwards optimization of the different components amounts as well as buffer pH and incubation time was needed.

2.5. Optimization of peroxidase mimetic activity of Cu-MOF@GO nanozyme

Preliminary experiments were done at constant H_2O_2 concentration to optimize five factors. The first one if buffer pH where it was found that acidic pHs produce better absorbance. The second factor is OPD concentration where concentrations less than 30 mM gave optimum absorbance. The third one is nanozyme concentration where concentrations less than 2 mg

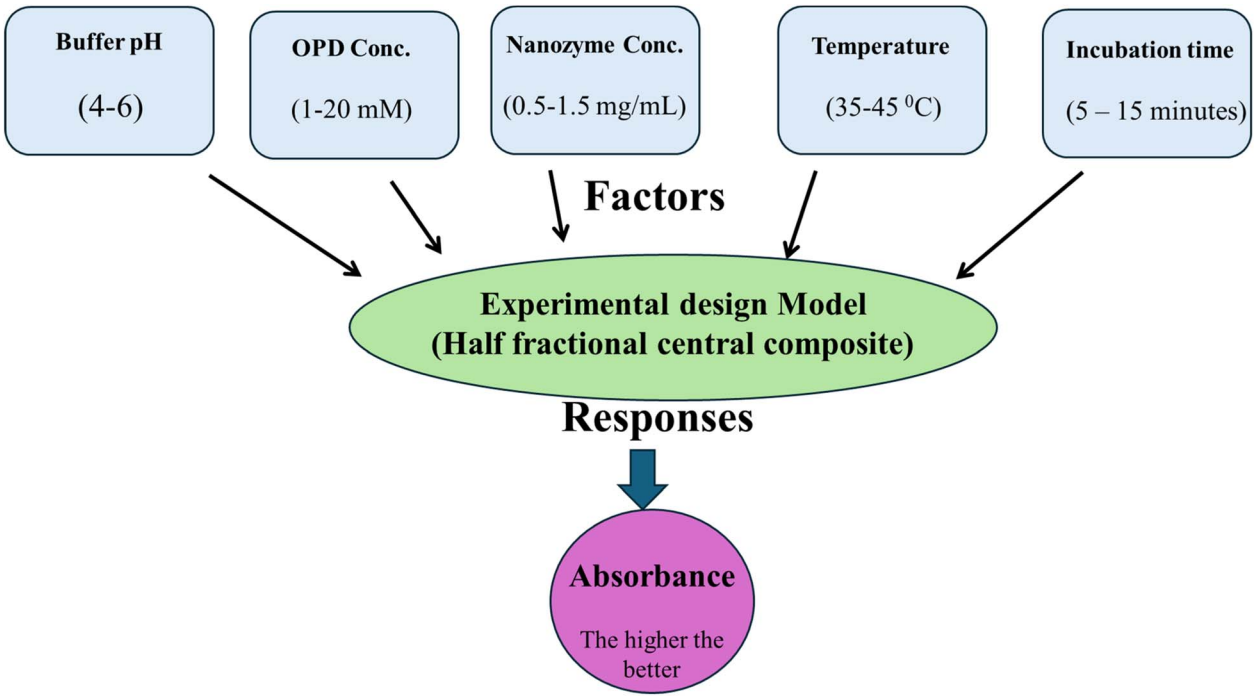

Fig. 1 Diagram of the experimental design showing the five factors tested and the measured response.

ml^{-1} showed enhanced absorbance signals. The fourth factor is temperature where temperature lower than 50 are found optimum to allow almost complete OPD oxidation. The fifth factor is incubation time where we found that beyond 15 min results are plateaued.

After preliminary experiments, quality by design (QbD) was utilized to further optimize each of the five factors. Surface response methodology was adopted; half factorial central composite design was utilized to optimize the five mentioned factors where 32 runs were implemented practically to find the optimum level for each factor. Only one response was measured, which is absorbance, the higher resulting absorbance the better. Fig. 1 shows the five factors with highest and lowest levels and the measured response.

2.6. Construction of calibration curve for determination of H_2O_2

Different concentrations of H_2O_2 were tested using the optimum experimental conditions obtained from the central composite model for the reaction between hydrogen peroxide and OPD catalyzed by the prepared Cu MOF@GO. The same procedure mentioned earlier under Section 2.4 was utilized, where absorbance was measured at 450 nm and calibration curve was constructed.

2.7. Characterization of the Cu-MOF@GO nanozymes

The EDX spectrum was utilized to determine the present elements and purity. The surface morphology and particle form were examined using a SEM microscopy. The interplay between chemical components and the alterations in the chemical constitution of the produced nanozymes were investigated using FTIR, while surface area and porosity were characterized using BET analysis.

2.8. Sarcosine detection using sarcosine oxidase (SOX) and the prepared nanozymes

Sarcosine oxidase 0.5 unit per ml prepared at pH 7 was added separately to sarcosine concentration 250 μM in an enzyme to substrate ratio (1 : 1 by volume), incubated at room temperature for 10 min 360 μL was withdrawn from this mixture (this reaction represents the source of H_2O_2) and added to 360 μL of 10 mM *O*-phenylenediamine and 10 μL of Cu-MOF@GO nanozyme (1 mg ml^{-1}), finally 2770 μL 0.2 M acetate buffer pH 4.0 was added. The resulting solution was put for 10 min into a 40 ° C water bath. The reaction was then assessed by measuring the absorbance of the oxidized OPD at 450 nm.

2.9. Optimization of the sarcosine measurement and calibration curve construction

In order to optimize the reaction between sarcosine and SOX, several factors were studied. These factors are, buffer pH, temperature and incubation time, ratio between SOX and Sar. After optimization different concentrations of Sar were analyzed using the exact previous procedure and absorbance was measured at 450 nm to construct Sar calibration curve.

2.10. Portable Arduino dependent RGB analysis

An extremely sensitive RGB sensing platform connected to an Arduino microcontroller was developed and constructed for portable, on-site quantification of H_2O_2 and sarcosine. The

device offers the same optical capabilities as a conventional spectrophotometer, but with small, inexpensive, and portable components. It consists of five main elements: a monochromatic light source (450 nm), which provides consistent excitation; a 3D printed cuvette holder, utilizing an ELEGOO Neptune 3 printer (Egypt); the cuvette holder had two orthogonal openings, one on the top to allow light to enter, and one on the side so that the transmitted signal could be detected at a 90° angle; an RGB color sensor (TCS34725-3.8 M:1, HiLetgo, China) used as the detector to capture the transmitted light intensity; and an Arduino Nano 3.0 microcontroller (USA), which handles the sensor output and calculates its absorbance. The processed data was presented on either a laptop or smartphone using a mini-USB or USB OTG connection, and this connection also provided power to the system. In this specific configuration, only the blue channel was monitored as this signal showed the most change as the concentration of the analyte increased. Overall, this setup was adapted from the portable design developed by Jun-Jie Poh *et al.*[36]

3. Results

The early and effective diagnosis of disease biomarkers relies on the accurate and timely detection of their concentrations for effective treatment to improve patient outcomes. The proposed work focuses on the determination of the prostate cancer biomarker, sarcosine. In this context, nanozymes possessing intrinsic enzyme-mimicking catalytic activity-have emerged as a powerful alternative to natural enzymes by offering high stability, tunable activity, and cost-effective synthesis. In light of these advantages, this study has focused on designing and optimizing a nanozyme comprising a Cu-MOF@GO nanozyme, exhibiting an improved peroxidase-like activity, for sensitive colorimetric detection of hydrogen peroxide and sarcosine. As mentioned earlier, under introduction the cascade reaction involves two steps, step one is the sarcosine reaction with SOX to produce H_2O_2 and step two where the produced H_2O_2 oxidizes the OPD substrate into the DAP yellow solution. So, this produced yellow colour corresponds to H_2O_2 concentration which is related to the sarcosine concentration. Results are structured starting with Step two optimization, application and validation to determine H_2O_2. Then after establishing the peroxidase mimic activity, well designed structural characterization is discussed to understand the shape, pore size, surface area and composition of the prepared nanozyme is described to relate the chemistry to prepared nanozyme performance. Discussion is then established for the optimization, application and validation of the nanozyme to determine sarcosine biomarker. Finally, selectivity study, reproducibility study and comparison with previously reported colorimetric sensors are presented.

3.1. Colorimetric detection of H_2O_2

Hydrogen peroxide is an important molecule in many areas of biology, such as screening for disease and pollution tracking. It is a sign of oxidative stress that is connected to a number of disorders, including malignancy, nervous system disturbances, and problems with the heart and blood vessels. This makes H_2O_2 useful for finding tissue collapse and keeping track of how a disease is getting worse. The reaction is composed of the prepared nanozyme which acts as peroxidase like catalyst, this catalyst facilitates the reaction between H_2O_2 (target analyte) and OPD substrate to yield the DAP yellow colour whose intensity corresponds to H_2O_2 concentration. The reaction needs control over the OPD concentration, nanozyme concentration, temperature, pH and time which are optimized in the following section. The proposed mechanism for the peroxidase-like activity of the nanozymes reaction with H_2O_2 and OPD proceeds in the following steps.[69] First, H_2O_2 molecules adsorb on the nanozyme surface, often binding to surface metal sites. Second, surface metal sites transfer electrons to H_2O_2, which breaks the O–O bond. Third, homolytic cleavage of H_2O_2 produces $OH^{\bullet}$ radicals, which then oxidize substrates like OPD to produce a colorimetric signal.[70,71] The assay is based on the direct and proportional correlation of H_2O_2 concentration and the catalytic oxidation of OPD, mediated by Cu-MOF@GO nanozymes. Here H_2O_2 represents the target analyte whose concentration will correlate with sarcosine determination in the following subsections. The method demonstrated outstanding analytical performance, where the absorbance spectrum exhibited a gradual increase across a wide concentration range of 0.5 μM to 1 mM H_2O_2, Fig. S1B. The proposed nanozyme sensor was utilized to construct a very linear calibration curve within this range, yielding a correlation coefficient (R) of 0.9998, with a low detection limit (LOD) of 0.17 μM. The data collected reinforces the feasibility of the synthesized nanozymes for development of an accurate and low-cost point-of-care system for H_2O_2 detection.

3.2. Optimization of peroxidase mimic action of Cu-MOF@GO nanozymes

A half-fractional Central Composite Design (CCD) was employed to optimize the catalytic performance of the Cu/GO nanozyme for the reaction with H_2O_2 by evaluating the combined effects of five key factors: buffer pH, OPD concentration, nanozyme concentration, reaction temperature, and incubation time as presented in Table S1. This design allowed the exploration of both linear and quadratic interactions among variables using only 32 experimental runs instead of the full factorial $2^5 = 243$ possible combinations, thus significantly reducing experimental effort and material consumption.[72–74] Measured absorbance values range from 0.43 to 1.12, which reflect the nanozyme's peroxidase-like activity under different conditions. It can be observed that the reaction efficiency is sensitive to the interactions between pH and substrate concentration and also to catalyst dosage and temperature. The maximum absorbance of 1.12 was obtained near the center point conditions: pH 4.0, OPD 10.5 mM, nanozyme 1.5 mg ml^{-1}, 40 °C, 10 min, which means an optimum balance between the substrate available and catalytic surface activity. This result was confirmed by the desirability diagram in Fig. S2 and optimum absorbance Fig. S3. Lower or higher pH values

resulted in decreased absorbance due to reduced enzyme-like stability or substrate ionization effects.

The use of a fractional CCD provided several advantages: it enabled the identification of significant factors and their interactions with high statistical confidence, minimized the number of experiments while maintaining model accuracy, and produced reliable response surface and contour plots to visualize optimal conditions. This approach is especially advantageous when dealing with nanozyme systems, where a variety of synthesis and/or operational parameters can nonlinearly affect catalytic efficiency.

3.3. Validation of the proposed method for determination of H_2O_2

The presented analytical technique was validated according ICH regulations.[75] Specificity is discussed in detail under Section 3.9. The accuracy of the proposed method was evaluated by analyzing three concentration levels of standard hydrogen peroxide solutions (1, 50, and 600 μM). Each concentration was measured in triplicate (nine determinations in total), and the mean recovery percentage (R%) was calculated to assess method accuracy, yielding an average of 99.86% ± 0.59 Table 1. The assay was evaluated for precision at two levels: intraday precision (repeatability) and interday precision (intermediate precision). For intraday precision, the same three concentration levels were measured three times in one day. For inter-day precision, the measurements were replicated three times on separate days. In both intraday and inter-day measurements, acceptable relative standard deviation (RSD%) values supported the reproducibility of the method Table 1. The linearity of the method was assessed over the concentration readings of 0.5–1000 μM H_2O_2, with good calibration curve and regression equation produced Fig. S1A. The detection limit (DL) and the quantification limit (QL) were calculated using the standard deviation (SD) of the response and the slope of the calibration curve (m) with the equations LOD = 3.3 (SD/m) and LOQ = 10 (SD/m). Based on the equations, the values obtained were 0.17 μM and 0.499 μM, respectively Table 1. Robustness was also evaluated by making small intentional changes to specific experimental conditions: buffer pH, temperature, incubation time, and catalyst concentration. The RSD% values observed were low Table 2, supporting the reliability and stability of the developed colorimetric sensor.

Table 2 Robustness of the proposed colorimetric method at fixed concentration 600.0 μM of H_2O_2

Parameter	Value	Absorbance			RSD %
Buffer pH	4.2	0.961	0.936	0.942	1.379
	3.8	0.992	1.01	1.03	1.881
Temperature (°C)	38	0.984	0.979	0.995	0.830
	42	1.03	1.01	0.994	1.783
Incubation time (minutes)	11	0.974	0.969	0.977	0.415
	9	0.996	1.01	1.02	1.195
Catalyst concentration (mg mL^{-1})	1.1	0.997	0.993	1.02	1.452
	0.9	0.975	0.968	0.966	0.487

3.4. Characterization of the fabricated Cu-MOF@GO nanozymes

The fabricated nanozymes were analysed using SEM-EDX, BET, FTIR and XRD analysis in order to understand how the structure, morphology and composition help to enhance the peroxidase like activity.

3.4.1. Scanning electron microscope and energy dispersive X-ray analysis SEM-EDX. Scanning Electron Microscopy (SEM) was used to examine the surface morphology and structural features of the Cu-MOF@GO nanozyme at a high resolution. This technique allows for the observation of the particle size, shape, and distribution of Cu-MOF crystals on the graphene oxide surface.[76] Energy Dispersive X-ray Spectroscopy (EDX) was performed to determine the elemental composition of the Cu-MOF@GO nanozyme. The low-magnification overview, Fig. 2A reveals a robust and homogeneous distribution of bright Cu-MOF crystallites anchored across the darker, wrinkled, and layered framework of the graphene oxide (GO) support. The figure highlights the high compositional contrast between the metallic MOF nodes and the carbonaceous scaffold, confirming that the catalytic centers are effectively dispersed without significant bulk aggregation. At high resolution, Fig. 2B, the distinct polyhedral morphology of the Cu-MOF crystallites is

Table 1 Assay and validation parameters obtained for determination of H_2O_2 and sarcosine by the proposed colorimetric method

Parameter	H_2O_2	Sarcosine
Linearity range (μM)	0.5–1000	0.05–250
Slope	0.1813	0.006
Intercept	0.0015	0.197
Correlation coefficient (r)	0.9998	0.999
Accuracy (mean ± SD)	99.86 ± 0.59[a]	98.74 ± 0.88[b]
LOD (μM)	0.17	0.016
LOQ (μM)	0.499	0.051
Precision (%RSD)		
Intraday precision (repeatability)[c]	0.758	0.861
Interday precision (intermediate precision)[d]	1.662	1.921

[a] Average of three replicates for each of three concentrations (1, 50, 600 μM H_2O_2). [b] Average of three replicates for each of three concentrations (0.1, 50, 200 μM sarcosine). [c] Intraday precision (repeatability): measuring three concentrations (n = 3) each one measured three times in the same day. [d] Interday precision: measuring three concentrations (n = 3) each one measured three times in different days.

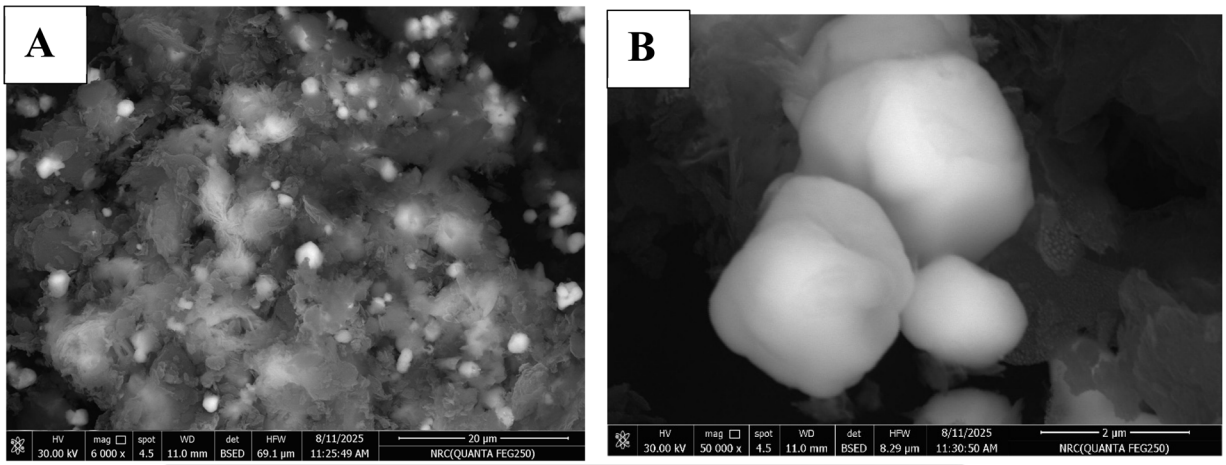

eZAF Smart Quant Results

Element	Weight %	Atomic %	Net Int.	Error %	Kratio	Z	A	F
C K	35.28	68.31	141.67	10.21	0.1035	1.1740	0.2498	1.0000
O K	7.36	10.69	56.91	12.77	0.0174	1.1284	0.2097	1.0000
CuK	57.36	20.99	497.56	2.90	0.4924	0.8456	1.0095	1.0057

Fig. 2 SEM images of Cu-MOF@GO (A) low-magnification images showing MOF particles anchored on wrinkled GO surfaces (B) high magnification image show the polyhedral shape of the prepared MOF (C) EDX elemental map overlay showing homogeneous distribution of Cu over carbon-rich GO.

clearly visible, featuring well-defined octahedral facets characteristic of a highly crystalline HKUST-1 type framework.[77,78] These crystallites exhibit a narrow, nanoscale size distribution ranging from 200 to 500 nm, which provides a high surface-to-volume ratio for catalytic turnover. The intimate interfacial contact between these faceted particles and the GO ripples suggests a strong structural anchoring, which is essential for facilitating rapid electron transfer during the peroxidase-mimetic redox cycle.[79]

The elemental purity and quantitative distribution of the composite were further validated by EDX analysis Fig. 2C. The spectrum identifies copper (Cu) as the dominant metallic phase (57.36% by weight), representing the active catalytic sites responsible for the decomposition of H_2O_2. Carbon (C) and oxygen (O) account for 35.28% and 7.36% of the weight, respectively, corresponding to the organic trimesic acid linkers and the functionalized GO support. The absence of exogenous elemental peaks confirms the success of the solvothermal synthesis and ensures that the observed peroxidase-like activity is intrinsically derived from the Cu-MOF@GO architecture.

3.4.2. Brunauer–Emmett–Teller (BET) analysis. Brunauer–Emmett–Teller (BET) surface area analysis was conducted to measure the specific surface area of the Cu-MOF@GO nanozyme. This technique provides valuable information about the material's porosity and surface characteristics, which are important for understanding its catalytic performance and adsorption capacity.[80] The permanent porosity and structural architecture of the Cu-MOF@GO nanozyme were quantified *via* N_2 adsorption–desorption isotherms at 77.35 K. As illustrated in Fig. S4, the material exhibits a type IV isotherm profile featuring a distinct H3-type hysteresis loop. The presence of the H3 loop, which remains open until moderate relative pressures (P/P_0 0.45), is a definitive physical signature of a hierarchical porous system containing slit-shaped pores.[81] These slit-like voids are not intrinsic to the bulk MOF but arise specifically from the interfacial assembly of polyhedral MOF crystallites within the non-rigid, plate-like layers of the graphene oxide (GO) matrix.[82] The calculated Brunauer–Emmett–Teller surface area is 1476.8 $m^2\ g^{-1}$, showing a highly porous structure with a great number of accessible active sites. C constant of 30.7 indicates medium nitrogen–surface interaction, while its correlation coefficient (r

= 0.9974) confirms the accuracy of BET fitting. This value is characteristic of a well-developed HKUST-1 ($Cu_3(BTC)_2$) framework and confirms that the MOF's internal structure remained intact and fully accessible after hybridization with GO, The structure consists of copper paddle-wheel clusters coordinated by benzene-1,3,5-tricarboxylic acid (trimesic acid) linkers, forming a face-centered cubic lattice with high intrinsic porosity.[77,78] The total pore volume was determined to be 0.1983 $cm^3\ g^{-1}$, further supporting the highly porous nature of the nanocomposite. To further explore the pore architecture, the Pore Size Distribution (PSD) was derived using the BJH (Barrett–Joyner–Halenda) model applied to the adsorption branch Fig. S5. The distribution identifies an average pore radius of 1.4161 nm, primarily falling within the transition region between large micropores and small mesopores.[83] This hierarchical porosity is functionally significant for the sensing mechanism: the smaller pores provide the high-energy environments for the peroxidase-mimetic H_2O_2 decomposition, while the larger mesoporous channels (extending up to 60.0 nm) act as mass-transport "highways" for the rapid diffusion of the sarcosine substrate and the bulky colorimetric intermediates. This dual-scale porosity is the fundamental reason for the rapid response and low detection limits observed in the analytical trials. The high surface area combined with narrow pore channels suggests that Cu-MOF crystals are well-developed and homogeneously distributed on the graphene oxide support, thus providing abundant catalytic centers and fast mass transport pathways for peroxidase-like activity and sensitive colorimetric detection.[82]

3.4.3. Fourier transform infrared analysis (FTIR). Fourier Transform Infrared Spectroscopy (FTIR) was employed to investigate the functional groups present in the Cu-MOF@GO nanozyme. This technique helps to identify the specific bonding interactions between the Cu-MOF and graphene oxide, particularly the presence of hydroxyl, carboxyl, and epoxide groups on the graphene oxide surface.[84] The FTIR spectrum of the Cu/GO composite Fig. S6 shows characteristic vibrational features confirming the successful integration of copper species with graphene oxide. The broad absorption band between 3400 and 3500 cm^{-1} corresponds to O–H stretching vibrations from the carboxylic group of trimesic acid, confirmed by the signal near 1720 cm^{-1} is appointed to C=O stretching of carboxylic group. The band observed at approximately 1620 cm^{-1} originates from C=C stretching within the sp^2 carbon of the graphene, indicating partial restoration of conjugated structure after the deposition process.[85] Peaks appearing around 1100–1200 cm^{-1} correspond to C–O and C–O–C vibrations of epoxy and alkoxy groups remaining on the GO surface.

3.4.4. X-ray diffraction analysis (XRD). X-ray Diffraction (XRD) analysis was performed to determine the crystallinity and phase composition of the Cu-MOF@GO nanozyme. This technique identifies the diffraction patterns of the crystalline phases present in the material.[86] The analysis revealed prominent diffraction peaks at 2θ = 36.63°, 43.55°, and 50.66°, which correspond to the copper (Cu) phase, with the peak at 43.55° showing the highest intensity as shown in Fig. S7 These peaks confirm the presence of crystalline copper, which is the primary component of nanozyme.[87] Additionally, a peak at 2θ = 26.66° was observed, corresponding to graphite (C6), indicating that graphene is also incorporated in the material.[88] A further diffraction peak at 2θ = 74.31° was attributed to Cuprite (Cu_2O), a copper oxide phase this may be formed by some sort of interaction between the Cu, GO and the trimesic acid. The relative intensities of these peaks, particularly the dominance of copper, highlight the material's significant copper content, which plays a crucial role in the catalytic activity of the nanozyme. The observed XRD pattern was compared to standard reference patterns from the ICDD database (reference codes: 96-

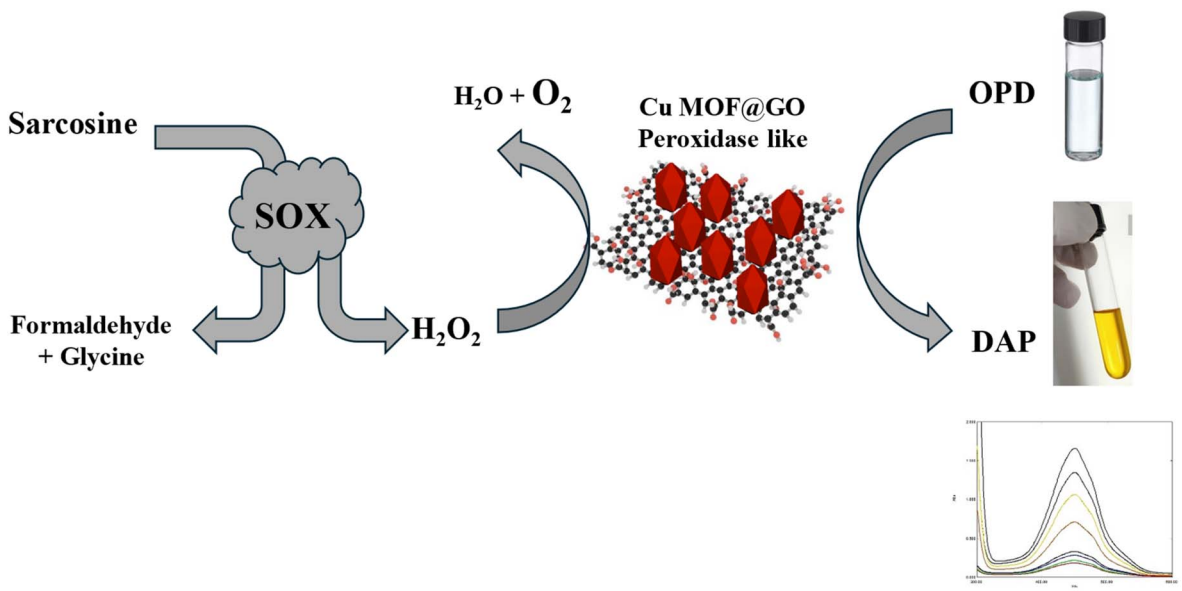

Scheme 1 Schematic illustration of sarcosine determination using the synthesized Cu-MOF@GO nanozymes.

901-1605 for Cu, 96-901-2706 for graphite, and 96-101-0964 for Cu_2O), further confirming the crystalline phases present in the prepared nanozyme.[89] These findings suggest that the Cu-MOF@GO nanozyme consists of a well-defined crystalline copper phase, with graphene and Cu_2O contributing to the material's overall structure and potential catalytic properties.

3.5. Determination of sarcosine using sarcosine oxidase and the prepared Cu MOF@GO nanozymes

Sarcosine (Sar) recently emerged as a promising metabolic biomarker strongly associated with prostate cancer progression and metastasis.[90,91] In this work, sarcosine was determined through a colorimetric assay that integrates the oxidative function of sarcosine oxidase (SOX) with the peroxidase-like catalytic activity of the synthesized nanozyme Cu-MOF@GO for the mediation of OPD oxidation in the presence of H_2O_2. The detection was performed in two successive steps as explained in the experimental section. First, the enzymatic oxidation of sarcosine in the presence of SOX (0.5 U per ml) was performed at room temperature in 0.2 M phosphate buffer, pH 7.0, for 15 min, using a 1 : 1 ratio between SOX and sarcosine. This resulted in the production of hydrogen peroxide proportional to the concentration of sarcosine stoichiometrically Scheme 1. Further on, the produced H_2O_2 was spectrophotometrically determined at 450 nm through its catalytic oxidation of OPD by Cu-MOF@GO nanozyme. A sensitive colorimetric response resulted from this and was directly related to the concentration of sarcosine.

3.6. Optimization of sarcosine reaction with sarcosine oxidase and construction of calibration curve

In order to optimize reaction between sarcosine and sarcosine oxidase five factors were studied. The first factor is SOX concentration, different concentrations were trialed (0.1–1 Unit per ml), where 0.5 Unit per ml showed optimum response Fig. S8A. The second factor is pH, different pHs were trialed (5, 6, 7, 8, 9), where pH 8 produced higher signal for the reaction between SOX and Sar Fig. S8B. The third factor is ratio between SOX and Sar, different ratios were experimented (1 : 1, 1 : 2, 1 : 3, 3 : 1 SOX to Sar) where 1 : 3 ratio showed better sensor performance Fig. S8C. The fourth and fifth factors are reaction temperature and times, where various values were experimented (25, 30, 35, 40 °C for temperature and 5, 10, 15, 20 min for time) where 10 min at room temperature showed highest absorbance readings Fig. S8D and S8E. Afterwards different controls for this experiment were prepared to ensure that the measured signal corresponds to H_2O_2 produced from the reaction between SOX and Sar. Also to ensure that the PAD colour production is only due to action of H_2O_2 on OPD in presence of the prepared Cu MOF@GO nanozyme. Results presented in Table S2 Shows that OPD with SOX and Sar without the nanozymes, cannot oxidize OPD. This means that the

Table 3 Studying the sensing performance of the proposed colorimetric method for H_2O_2 and sarcosine determination using OPD substrate and Cu-MOF@GO nanozymes compared to other reported nanomaterials

Material/sensing system	Analyte	Linear range (μM)	LOD (μM)	References
Metformin–Zn–Thiourea	H_2O_2	10–800	2.97	18
	Sarcosine	Not tested	Not tested	
Ni/Co-MOF@CMC	H_2O_2	10–800	3.28	19
	Sarcosine	Not tested	Not tested	
2D Co-MOF nanosheets	H_2O_2	5.0–200	4.60	20
	Sarcosine	Not tested	Not tested	
Photothermal biosensing integrated with microfluidic paper-based analytical device (PT-μPAD)	H_2O_2	Not found	Not found	21
	Sarcosine	0.01–0.04	0.000032	
Paper-based polyallylamine hydrochloride (PAH) sensor	H_2O_2	Not found	Not found	22
	Sarcosine	0.6–10	0.6	
Paper-based HRP/UiO-66	H_2O_2	Not found	Not found	23
	Sarcosine	8–400	5.0	
HRP mimic peptide	H_2O_2	Not found	Not found	24
	Sarcosine	0.25–200	Not specified	
Carbon QDs/AuNRs	H_2O_2	Not found	Not found	25
	Sarcosine	0.02–1.0	0.011	
$(Cu_3(PO_4)_2$:Ce@SOX)	H_2O_2	10–300	3.4	26
	Sarcosine	1.0–50	0.38	
$Fe_3O_4@SiO_2@NiCo_2S_4$	H_2O_2	2.5–800	0.87	27
	Sarcosine	1.25–350	0.42	
Folate functionalized polyoxometalate	H_2O_2	5–100	0.21	28
	Sarcosine	5–100	0.34	
Fe-doped g-C_3N_4 nanoflakes	H_2O_2	2–100	1.8	29
	Sarcosine	10–500	8.6	
O_3-CDs	H_2O_2	1.0–100	0.46	14
	Sarcosine	2.0–100	1.1	
Cu-MOF@GO	H_2O_2	0.5–1000	0.15	Current work
	Sarcosine	0.5–250	0.16	

presence of Cu MOF/nanozymes is crucial for the peroxidase activity. Another observation is that nanozymes without SOX did not give signal which means that the synthesized nanozymes have only peroxidase like activity not oxidase activity.

The proposed method was validated for the determination of sarcosine as per ICH guidelines.[75] In order to construct the calibration curve, a set of sarcosine solutions with different concentrations were prepared and assessed. It was determined that there was a straight-line relationship present from 0.05 to 250 μM, with a detection limit of 0.016 μM, and R^2 of 0.999 Fig. S9A. The Arduino setup mentioned earlier is presented in is presented in a schematic view in Fig. S9B. The corresponding spectra to the colors measured indicated a gradual increase in absorbance intensity with increasing sarcosine concentration. As the amount of the oxidized (OPD) product is directly related to the H_2O_2 produced, which correlates with sarcosine concentration, the colorimetric response can reliably be used for quantification. These obtained results showed good accuracy and precision as presented in Table 1. The data verify the high sensitivity of the colorimetric nanozyme integrated method developed for measuring sarcosine.

3.7. Comparison with previously reported methods

The sensing capability utilizing the method was compared against other nanomaterials reported in the literature[14,18–29] as shown in Table 2. The reported methods are newly synthesized catalysts with peroxidase like activity for determination of H_2O_2 and/or sarcosine, all of them show good performance and advanced characterization, however most of them show narrow linearity range and most of them handle validation parameters for one analyte either H_2O_2 or sarcosine. On the other hand, the reported methods characterizing both H_2O_2 and sarcosine show relatively lower sensitivity. The presented colorimetric technique exhibits both exceptional sensitivity (lower detection limit) and wider linearity range regarding determination of both H_2O_2 and sarcosine, which is highly advantageous over previously reported techniques. These exceptional analytical results may be attributed to the unique design of the proposed sensor, extending the catalytic activity of Cu through the linkage with GO. In addition, careful and computational optimization through the CCD model allowed perfection of the critical parameters affecting measurement of both H_2O_2 and sarcosine. Finally, the application of the Arduino based device for onsite colorimetric determination boosts and widens the applicability of the proposed sensor (Table 3).

3.8. Selectivity study

Selectivity offers a great challenge Cu MOF@GO based colorimetric sensor, because almost all biological samples contain amino acids that can interfere with sarcosine. The proposed method has unique selectivity to sarcosine determination in real samples for two reasons. The first one is the exceptional specificity between sarcosine oxidase enzyme (from bacillus) and sarcosine. The second reason is the optimized experimental conditions for sarcosine analysis which make the prepared nanozyme, smart nanomaterials that are activated only in certain conditions. Selectivity was studied using the very structurally related amino acids (glycine, methyl alanine). Formaldehyde, which is the product of sarcosine oxidation, is also a possible interferent. Glucose and uric acid are common substrates in the human body that have their own oxidase enzyme. Finally, creatinine that is present in heavily in urine samples and to limited extent in serum. Results plotted in Fig. 3 show the unique selectivity of the proposed method to sarcosine.

3.9. Application of the colorimetric analysis for quantifying sarcosine in real samples

Serum of healthy individuals was purchased from VACCERA. Sample was diluted (1 : 1) with phosphate buffer pH 8, then a specified volume from dilution was mixed at the optimum ratio with 0.5 Unit per ml SOX and left for 10 min at room

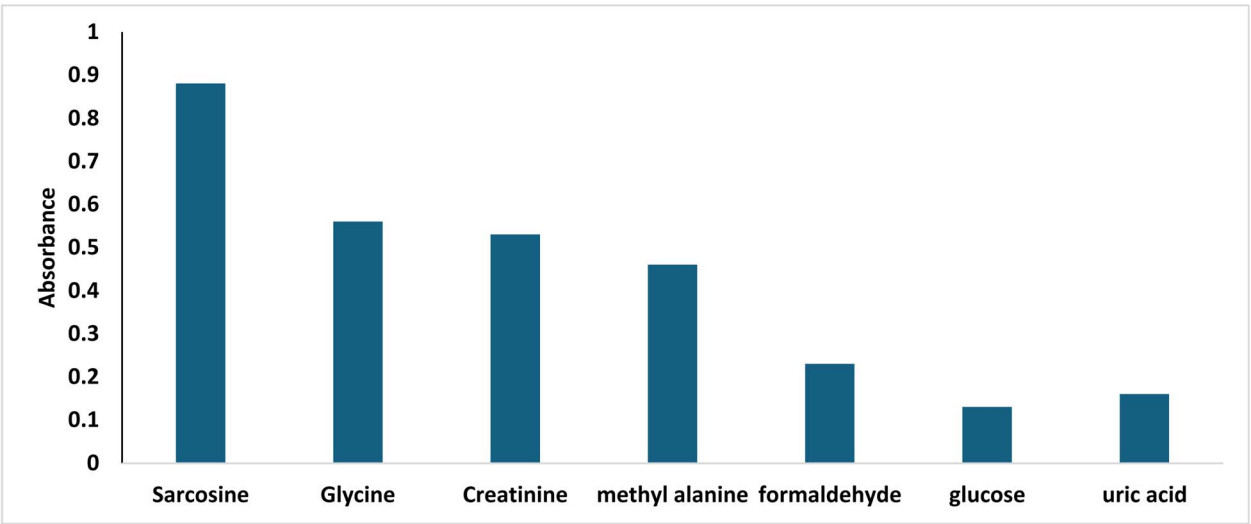

Fig. 3 Selectivity study for the proposed nanozyme based colorimetric sensor for the determination of sarcosine.

Table 4 Determination of sarcosine in spiked human serum samples ($n = 3$)

Sample	Added μM	Found conc. (μM) ± SD	Recovery%
Healthy human serum	0	2.10 ± 0.96	—
samples	20	19.63 ± 1.55	98.15
	100	98.50 ± 0.62	98.50
Mean ± SD			98.33 ± 0.25

Table 5 Determination of sarcosine in spiked human serum samples using the proposed method in comparison with commercial kit

	Sarcosine concentration (μM)	
	Proposed assay[a]	Commercial laboratory kit[b]
Sample	R% ± SD	R% ± SD
Healthy human serum samples spiked with 80 μM sarcosine	100.81 ± 0.93	100.64 ± 0.67
n	3	3
Variance	0.865	0.449
Student's t-test (2.776)	0.26	—
F Value (19)	1.93	—

[a] $n = 3$. [b] Abcam® (cat no. ab65338), UK.

temperature. Afterwards 360 μL of the mixture were added to 360 μL of 10 mM OPD and 10 μL of 1 mg per ml Cu MOF@GO and 2770 μL acetate buffer pH 4. The final solution was kept at 40 °C for ten min. and the absorption of the produced solution was analysed at 450 nm. Sarcosine concentration will be calculated from the regression equation of calibration curve. Spiked serum samples with standard sarcosine were analyzed for comparative purposes (Table 4). In order to assess the accuracy and practicality of the method, the outcomes of the suggested colorimetric assay were contrasted with those of a sarcosine detection kit that was sold commercially (Table 5). Results showed that the proposed colorimetric assay can quantitatively determine sarcosine in serum with accepted accuracy and precision in the normal range as well as cases of prostate cancer.[92]

3.10. Determination of sarcosine using Arduino device for onsite analysis

While high-precision spectrophotometry validates the fundamental catalytic performance of the Cu-MOF@GO nanozyme, the practical utility of a diagnostic tool—especially for prostate cancer screening—depends on its accessibility in resource-limited settings. To demonstrate the "Point-of-Care" (PoC) potential of our platform, we integrated the colorimetric assay into a custom-engineered portable analytical setup. Unlike traditional laboratory instrumentation, this system utilizes a low-cost TCS34725 RGB color sensor interfaced with an Arduino Nano microcontroller to perform real-time, on-site analysis.[93] Previous studies have confirmed the quantitative assessment of various analytes, including sarcosine, nickel, and iron, through the use of RGB color sensors.[62,93,94] The detection principle relies on the digital quantification of the color transition from colorless to yellow (DAP). As the sarcosine concentration increases, the intensity of the yellow product rises, causing a systematic and measurable decrease in the blue channel response of the RGB sensor. This inverse correlation was calibrated to match the optical absorbance trends observed in spectrophotometric trials. As shown in Fig. 4, the resulting calibration curve demonstrates a high degree of linearity, proving that our nanocomposite maintains its ultra-sensitive detection capabilities even when transitioned to a simplified, portable electronic interface. By bypassing the need for advanced laboratory infrastructure, this Arduino-based setup transforms the Cu-MOF@GO nanozyme from a benchtop material into a viable clinical tool for rapid, decentralized biomarker monitoring.

3.11. Evaluation of the reproducibility and operational stability of the Cu-MOF@GO nanozyme for reliable sarcosine quantification

The Cu-MOF@GO nanozyme was evaluated for its reproducibility and stability over time. Reproducibility was evaluated by measuring sarcosine at 5.0 μM, 80.0 and 200.0 μM, utilizing three individual sensors made on same day. Then, evaluation of the same two concentrations levels using three sensors that have been prepared on three different days. The relative standard deviations for intrabatch and interbatch preparation were calculated for each sensor and all were less than 2% RSD, indicating reproducibility of fabrication and performance, results are presented in Fig. S10A and S10B. Long-term stability of the Cu-MOF@GO nanozyme was assessed for one sensor at the same three levels of sarcosine over a period of six months. During this period, two sensors were also evaluated for the consistent catalytic activity of the nanozyme when OPD

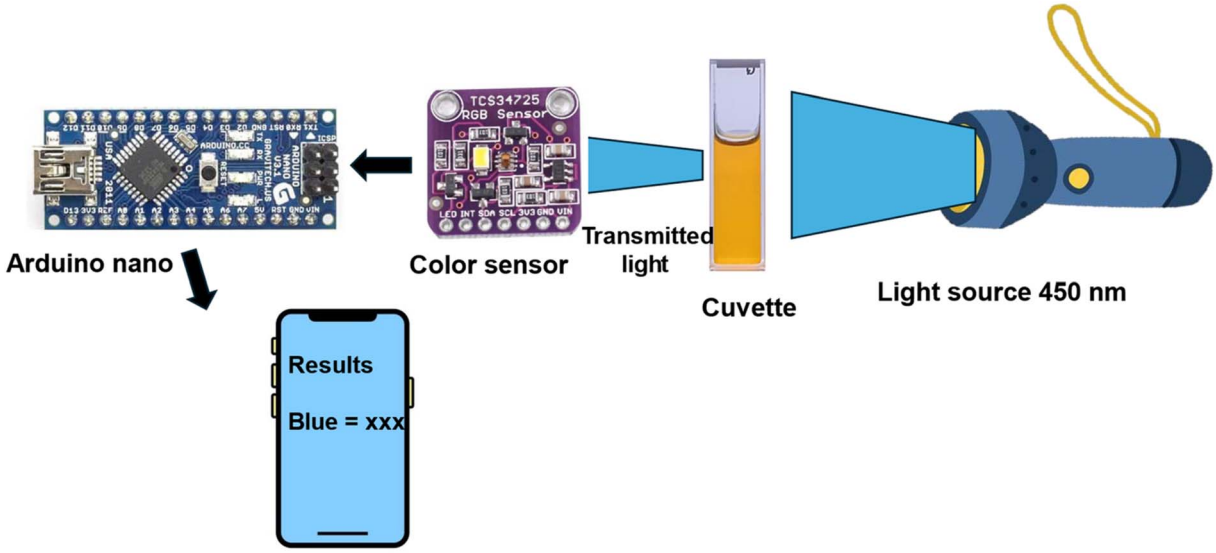

Fig. 4 Diagram of the Arduino based portable device.

substrate was oxidized with H_2O_2 over six-month period, where also satisfactory RSD % were obtained. What these quantitative and qualitative results showed, was that the Cu-MOF@GO nanozyme has good structural stability and catalytic stability for biosensing applications which demonstrates reliability and durability for sarcosine detection in real-world diagnostic testing application.

4. Conclusion

Novel Cu-MOF@GO was successfully synthesized and optimized as a high-performance peroxidase-like nanozyme for quantification of both H_2O_2 and Sar, a key biomarker associated with prostate cancer progression. The integration of statistical optimization by using a half-fractional CCD allowed for a systematic investigation of experimental factors, which greatly enhanced the catalytic efficiency and analytical response of this nanozyme. The optimized nanozyme showed wide linear ranges and low detection limits for both H_2O_2 and sarcosine, with superior performances compared to many previously reported colorimetric systems. Its excellent stability, reproducibility, and high recovery rates in spiked urine samples confirm the reliability and practical potential of the developed platform. Moreover, the effective combination of colorimetric assay with smartphone-based RGB analysis opens an interesting avenue toward portable, low-cost, and point-of-care diagnostics. This work not only presents a simple strategy for the design and optimization of nanozyme sensors but also contributes to advancing early, accessible prostate cancer screening through intelligent analytical design and nanomaterial engineering. Looking ahead, future research could focus on exploring this nanozyme potential in detecting a broader range of biomarkers. The integration of this nanozyme along with other sensors for other biomarkers into portable and low-cost diagnostic device could revolutionize point-of-care testing, particularly for early disease detection. Its high surface area, selectivity, and ease of functionalization suggest significant applications in medical diagnostics, environmental monitoring, and other areas requiring efficient, rapid detection of analytes.

Conflicts of interest

There are no conflicts of interest to declare.

Data availability

All data generated or analyzed during this study are included in the article [and/or its supplementary information (SI)]. Supplementary information is available. See DOI: https://doi.org/10.1039/d6ra01609j.

Acknowledgements

The authors gratefully acknowledge Professor Dr Marianne Nebsen and Associate Professor Dr Ahmed Hafez (Faculty of Pharmacy, Cairo University) for their valuable scientific input and for generously providing the sarcosine, sarcosine oxidase, and the commercial kit essential for this work.

References

1 J.-Y. Chen, P.-Y. Wang, M.-Z. Liu, F. Lyu, M.-W. Ma, X.-Y. Ren and X.-S. Gao, Biomarkers for Prostate Cancer: From Diagnosis to Treatment, *Diagnostics*, 2023, **13**, 3350, DOI: 10.3390/diagnostics13213350.
2 T. S. C. R. Rebelo, C. M. Pereira, M. G. F. Sales, J. P. Noronha, J. Costa-Rodrigues, F. Silva and M. H. Fernandes, Sarcosine oxidase composite screen-printed electrode for sarcosine determination in biological samples, *Anal. Chim. Acta*, 2014, **850**, 26–32, DOI: 10.1016/j.aca.2014.08.005.

3 J. McKiernan, M. Noerholm, V. Tadigotla, S. Kumar, P. Torkler, G. Sant, J. Alter, M. J. Donovan and J. Skog, A urine-based Exosomal gene expression test stratifies risk of high-grade prostate Cancer in men with prior negative prostate biopsy undergoing repeat biopsy, *BMC Urol.*, 2020, **20**, 138, DOI: 10.1186/s12894-020-00712-4.

4 M. Wang, L. Zhang, X. Zhou, J. Zhang, C. Zhou and X. Su, Fluorescence sensing platform for sarcosine analysis based on nitrogen-doping copper nanosheets and gold nanoclusters, *Anal. Chim. Acta*, 2022, **1223**, 340188, DOI: 10.1016/j.aca.2022.340188.

5 Y. Luo, J. Wang, L. Yang, T. Gao and R. Pei, In vitro selection of DNA aptamers for the development of fluorescent aptasensor for sarcosine detection, *Sens. Actuators, B*, 2018, **276**, 128–135, DOI: 10.1016/j.snb.2018.08.105.

6 R. Deswal, V. Narwal, P. Kumar, V. Verma, A. S. Dang and C. S. Pundir, An improved amperometric sarcosine biosensor based on graphene nanoribbon/chitosan nanocomposite for detection of prostate cancer, *Sens. Int.*, 2022, **3**, 100174, DOI: 10.1016/j.sintl.2022.100174.

7 P. Kumar, V. Narwal, R. Jaiwal and C. S. Pundir, Construction and application of amperometric sarcosine biosensor based on SOxNPs/AuE for determination of prostate cancer, *Biosens. Bioelectron.*, 2018, **122**, 140–146, DOI: 10.1016/j.bios.2018.09.003.

8 C. S. Pundir, R. Deswal and P. Kumar, Quantitative analysis of sarcosine with special emphasis on biosensors: a review, *Biomarkers*, 2019, **24**, 415–422, DOI: 10.1080/1354750X.2019.1615124.

9 V. Yamkamon, P. P. Yee, S. Yainoi, W. Eiamphungporn and T. Suksrichavalit, Simultaneous determination of sarcosine and its related metabolites by gas chromatography-tandem mass spectrometry for prostate cancer diagnosis, *EXCLI J.*, 2018, **17**, 965–979, DOI: 10.17179/excli2018-1352.

10 T.-C. Chung, C.-T. Li, H.-S. Kou and H.-L. Wu, High-Performance Liquid Chromatographic Analysis of Sarcosine as a Fluorescent Levofloxacin Derivative, *J. Chromatogr. Sci.*, 2015, **53**, 1310–1315, DOI: 10.1093/chromsci/bmv010.

11 P. A. Markin, A. Brito, N. Moskaleva, M. Fodor, E. V. Lartsova, Y. V. Shpot, Y. V. Lerner, V. Y. Mikhajlov, N. V. Potoldykova, D. V. Enikeev, A. V. Lyundup and S. A. Appolonova, Plasma Sarcosine Measured by Gas Chromatography-Mass Spectrometry Distinguishes Prostatic Intraepithelial Neoplasia and Prostate Cancer from Benign Prostate Hyperplasia, *Lab. Med.*, 2020, **51**, 566–573, DOI: 10.1093/labmed/lmaa008.

12 N. Jornet-Martínez, C. J. Henderson, P. Campíns-Falcó, R. Daly and E. A. H. Hall, Towards sarcosine determination in urine for prostatic carcinoma detection, *Sens. Actuators, B*, 2019, **287**, 380–389, DOI: 10.1016/j.snb.2019.02.061.

13 Z. Heger, N. Cernei, S. Krizkova, M. Masarik, P. Kopel, P. Hodek, O. Zitka, V. Adam and R. Kizek, Paramagnetic Nanoparticles as a Platform for FRET-Based Sarcosine Picomolar Detection, *Sci. Rep.*, 2015, **5**, 8868, DOI: 10.1038/srep08868.

14 W. Qin, H. Tian, Z. Meng, Z. Tang, J. Wang and Z. Wu, Facile synthesis and ozonation of carbon dots using mango pulps for dual-mode colorimetry and ratiometric fluorescence detection of sarcosine, *Microchem. J.*, 2023, **195**, 109468, DOI: 10.1016/j.microc.2023.109468.

15 Z. Ramezani, M. Safdarian and A. A. Ghadiri, Metal-coded hydrogel magnetic molecularly imprinted polymer for preconcentration and cleanup of sarcosine: Determination in urine; coupled to on-column capillary electrophoresis, *Talanta*, 2021, **230**, 122309, DOI: 10.1016/j.talanta.2021.122309.

16 J. Hu, W. Wei, S. Ke, X. Zeng and P. Lin, A novel and sensitive sarcosine biosensor based on organic electrochemical transistor, *Electrochim. Acta*, 2019, **307**, 100–106, DOI: 10.1016/j.electacta.2019.03.180.

17 B. Hengameh, M. Mousavi and S. Maghsoudi, Sensitive Voltammetric Method for Rapid Determination of Sarcosine as a New Biomarker for Prostate Cancer Using a TiO2 Nanoparticle/Ionic Liquid Modified Carbon Paste Electrode, *Russ. J. Electrochem.*, 2021, **57**, 149–158, DOI: 10.1134/S1023193521020099.

18 O. G. Hussein, A. M. Mahmoud, S. H. Ismail, A. Elshaer and N. Safwat, Silica-templated porous nanoparticles with multifunctional surface groups for sensitive colorimetric detection of glucose and hydrogen peroxide, *Microchem. J.*, 2025, **218**, 115552, DOI: 10.1016/j.microc.2025.115552.

19 Y. M. Abdelfattah, A. M. Mahmoud, N. I. Abdelaziz and D. A. El Mously, Point-of-care colorimetric biosensor for H2O2 and glucose detection utilizing the peroxidase-like activity of 2D bimetallic metal organic framework nanosheets, *Anal. Chim. Acta*, 2025, **1356**, 343993, DOI: 10.1016/j.aca.2025.343993.

20 A. A. Mouhamed, A. M. Mahmoud and D. A. El Mously, Point-of-care colorimetric biosensing using 2D Co-MOFs nanozymes for sensitive detection of glucose and hydrogen peroxide, *J. Anal. Sci. Technol.*, 2026, **17**, 8, DOI: 10.1186/s40543-025-00524-x.

21 K. Khachornsakkul and T. Leelasattarathkul, Photothermal biosensing integrated with microfluidic paper-based analytical device for sensitive quantification of sarcosine, *Talanta*, 2024, **271**, 125628, DOI: 10.1016/j.talanta.2024.125628.

22 M. Masumoto, S. Ohta, M. Nakagawa, Y. Hiruta and D. Citterio, Colorimetric paper-based sarcosine assay with improved sensitivity, *Anal. Bioanal. Chem.*, 2022, **414**, 691–701, DOI: 10.1007/s00216-021-03682-0.

23 X. Yang, C. Jin, S. Yang and M. Tian, Paper-based enzyme-linked biosensor combined with smartphone for simultaneous colorimetric sensing of xanthines and sarcosine, *Sens. Actuators, B*, 2024, **412**, 135849, DOI: 10.1016/j.snb.2024.135849.

24 Z. Ma, L. Yang, Y. Wang, M. Wang, W. Qi and Z. He, Construction and stabilization of a peptide-based peroxidase mimic for the colorimetric detection of uric acid and sarcosine, *Chem. Eng. J.*, 2021, **416**, 129149, DOI: 10.1016/j.cej.2021.129149.

25 B. Mbage, Y. Li, H. Si, X. Zhang, Y. Li, X. Wang, A. Salah and K. Zhang, Fabrication of folate functionalized polyoxometalate nanoparticle to simultaneously detect H2O2 and sarcosine in colorimetry, *Sens. Actuators, B*, 2020, **304**, 127429, DOI: 10.1016/j.snb.2019.127429.

26 Q. Zhong, X. Qin, C. Yuan, R. Shi and Y. Wang, Colorimetric determination of sarcosine in human urine with enzyme-like reaction mediated Au nanorods etching, *Microchem. J.*, 2021, **165**, 106120, DOI: 10.1016/j.microc.2021.106120.

27 P. Liu, Q. Sun, Z. Gai, F. Yang and Y. Yang, Dual-mode fluorescence and colorimetric smartphone-based sensing platform with oxidation-induced self-assembled nanoflowers for sarcosine detection, *Anal. Chim. Acta*, 2024, **1306**, 342586, DOI: 10.1016/j.aca.2024.342586.

28 X. Wang, M. Chen and L. Zhao, Development of a colorimetric sensing assay for ascorbic acid and sarcosine utilizing the dual-class enzyme activity of Fe3O4@SiO2@NiCo2S4, *Chem. Eng. J.*, 2023, **468**, 143612, DOI: 10.1016/j.cej.2023.143612.

29 X. Xi, X. Peng, C. Xiong, D. Shi, J. Zhu, W. Wen, X. Zhang and S. Wang, Iron doped graphitic carbon nitride with peroxidase like activity for colorimetric detection of sarcosine and hydrogen peroxide, *Microchim. Acta*, 2020, **187**, 383, DOI: 10.1007/s00604-020-04373-w.

30 Z. Mu, S. Wu, J. Guo, M. Zhao and Y. Wang, Dual Mechanism Enhanced Peroxidase-like Activity of Iron–Nickel Bimetal–Organic Framework Nanozyme and Its Application for Biosensing, *ACS Sustain. Chem. Eng.*, 2022, **10**, 2984–2993, DOI: 10.1021/acssuschemeng.1c07975.

31 Y. He, M. Feng, X. Zhang and Y. Huang, Metal-organic framework (MOF)-derived flower-like Ni-MOF@NiV-layered double hydroxides as peroxidase mimetics for colorimetric detection of hydroquinone, *Anal. Chim. Acta*, 2023, **1283**, 341959, DOI: 10.1016/j.aca.2023.341959.

32 P. K. Marvi, S. R. Ahmed, P. Das, R. Ghosh, S. Srinivasan and A. R. Rajabzadeh, Prunella vulgaris-phytosynthesized platinum nanoparticles: Insights into nanozymatic activity for H2O2 and glutamate detection and antioxidant capacity, *Talanta*, 2024, **274**, 125998, DOI: 10.1016/j.talanta.2024.125998.

33 M. N. Saad, A. M. Mahmoud, M. Wadie, S. M. Amer, I. M. El-Sherbiny and H. M. Marzouk, Computationally guided fabrication of chlorpyrifos electrochemical sensor based on molecularly imprinted polymer decorated with au nanoparticles, *Talanta Open*, 2025, **11**, 100457, DOI: 10.1016/j.talo.2025.100457.

34 M. N. Saad, H. M. Marzouk, S. M. Amer, I. M. El-Sherbiny and A. M. Mahmoud, Computationally Optimized Graphene-Based Electrochemical Sensor with Enhanced Signal Stability for the Determination of the Antimicrobial Agent 9-aminoacridine, *J. Electrochem. Soc.*, 2024, **171**, 107511, DOI: 10.1149/1945-7111/ad8522.

35 M. N. Saad, A. M. Mahmoud, S. M. Amer, I. M. El-Sherbiny and H. M. Marzouk, From food waste to water safety: mango endocarp-derived biogenic carbon dots as a fluorescent probe for real-time chlorine monitoring in pool water, *Environ. Sci.:Water Res. Technol.*, 2026, **12**, 727–741, DOI: 10.1039/D5EW00782H.

36 A. M. Saleh, O. Ramadan, A. M. Badawey, H. M. Marzouk, S. Cui and R. Y. A. Hassan, Nanostructured Biosensing Platforms for the Rapid Detection of Fungal Quorum-Sensing Molecules: Toward Early and Accurate Diagnosis of Candida albicans Infection, *ACS Infect. Dis.*, 2025, **11**, 3481–3490, DOI: 10.1021/acsinfecdis.5c00487.

37 E. A. Ibrahim, S. S. Saad, M. A. Hegazy, L. E. Abdel Fattah and H. M. Marzouk, A novel molecular imprinted polymer-based potentiometric sensor for determination of the neuromodulating drug safinamide in dosage form and biological fluids, *Microchem. J.*, 2025, **214**, 114059, DOI: 10.1016/j.microc.2025.114059.

38 O. G. Hussein, M. R. Rezk, A. M. Mahmoud and M. Wadie, Dual-sensor potentiometric platform utilizing β-cyclodextrin ionophores and Cu-gallic MOFs for ophthalmic drugs determination in rabbit aqueous humor, *Sens. Bio-Sens. Res.*, 2026, **52**, 101000, DOI: 10.1016/j.sbsr.2026.101000.

39 R. Abdullah, A. Sabry, A. M. Mahmoud and M. M. Galal, Smartphone-based colorimetric determination of dopamine using modified plasmonic gold nanoparticles via implementation of U2-net and machine learning algorithms, *Sens. Bio-Sens. Res.*, 2026, **52**, 100998, DOI: 10.1016/j.sbsr.2026.100998.

40 M. M. Elhassan, A. M. Mahmoud, M. A. Hegazy and S. Mowaka, A sustainable nanotechnology approach for finerenone detection using green-synthesized silver nanoparticles, *J. Nanopart. Res.*, 2026, **28**, 77, DOI: 10.1007/s11051-026-06577-2.

41 R. E. Bayoumy, N. A. El-Ragehy, N. Y. Hassan and A. M. Mahmoud, Development of a biosensor for spectrophotometric determination of l-lactate in artificial saliva, *BMC Chem.*, 2026, **20**, 39, DOI: 10.1186/s13065-025-01718-5.

42 O. G. Hussein, A. M. Mahmoud, M. K. A. El-Rahman and A. A. Mouhamed, Copper-carbidopa nanoparticles as highly active laccase-mimics for colorimetric detection and oxidative catalysis of o-phenylenediamine, *J. Anal. Sci. Technol.*, 2026, **17**, 13, DOI: 10.1186/s40543-026-00528-1.

43 A. M. Abdelfatah, K. A. M. Attia, E. A. El-Desouky, A. M. Mahmoud, A. El-Olemy and N. A. Abdelshafi, Eco-friendly differential pulse voltammetry for non-invasive detection of ofloxacin using zinc-based metal organic frameworks (Zn-MOF) with environmental sustainability assessment, *Microchem. J.*, 2026, **221**, 116770, DOI: 10.1016/j.microc.2025.116770.

44 Q. Zhang, S. Yan, X. Yan and Y. Lv, Recent advances in metal-organic frameworks: Synthesis, application and toxicity, *Sci. Total Environ.*, 2023, **902**, 165944, DOI: 10.1016/j.scitotenv.2023.165944.

45 Y. Chao, N. Deng and Z. Zhou, A review of recent advances in metal-organic frameworks materials for zero-energy passive adsorption of chemical pollutants in indoor environments, *Sci. Total Environ.*, 2024, **953**, 175926, DOI: 10.1016/j.scitotenv.2024.175926.

46 P. Arul, S.-T. Huang, C. Nandhini, C.-H. Huang, N. S. K. Gowthaman and C.-H. Huang, Development of a nanozyme-based electrochemical catalyst for real-time biomarker sensing of superoxide and nitric oxide anions released from living cells and exogenous donors, *Biosens. Bioelectron.*, 2024, **261**, 116485, DOI: 10.1016/j.bios.2024.116485.

47 S. N. Ali, A. M. Mahmoud, S. S. Saad, A. S. Fayed and H. M. Marzouk, A novel bimetallic metal–organic framework-based electrochemical nanosensor for therapeutic monitoring of meropenem in human plasma, *Microchem. J.*, 2025, **215**, 114184, DOI: 10.1016/j.microc.2025.114184.

48 A. M. Saleh, R. Y. A. Hassan, A. M. Badawey and H. M. Marzouk, Software-assisted evaluation of sustainable chemistry innovations: A critical analytical review of viability assays incorporating diseases' biomarkers with greenness, blueness, and whiteness computational metrics, *Microchem. J.*, 2025, **215**, 114437, DOI: 10.1016/j.microc.2025.114437.

49 A. M. Saleh, O. Ramadan, A. M. Badawey, H. M. Marzouk, S. Cui and R. Y. A. Hassan, Nanostructured Biosensing Platforms for the Rapid Detection of Fungal Quorum-Sensing Molecules: Toward Early and Accurate Diagnosis of Candida albicans Infection, *ACS Infect. Dis.*, 2025, **1**, 1–12, DOI: 10.1021/acsinfecdis.5c00487.

50 M. Sherazee, P. Khoshbakht Marvi, P. Das, S. Rahin Ahmed, S. Srinivasan and A. Reza Rajabzadeh, Silicene's intriguing nanozymatic activity: Improved colorimetric and electrochemically supported colorimetric biosensing, *Microchem. J.*, 2024, **201**, 110616, DOI: 10.1016/j.microc.2024.110616.

51 X. Niu, X. Li, Z. Lyu, J. Pan, S. Ding, X. Ruan, W. Zhu, D. Du and Y. Lin, Metal–organic framework based nanozymes: promising materials for biochemical analysis, *Chem. Commun.*, 2020, **56**, 11338–11353, DOI: 10.1039/D0CC04890A.

52 Y. Zhang, C. Zhang, W. Qian, F. Lei, Z. Chen, X. Wu, Y. Lin and F. Wang, Recent advances in MOF-based nanozymes: Synthesis, activities, and bioapplications, *Biosens. Bioelectron.*, 2024, **263**, 116593, DOI: 10.1016/j.bios.2024.116593.

53 J. Yu, Q. Sun, J. Sun, X. Wang, N. Niu and L. Chen, Development of gold nanoparticles composite functionalized bimetallic metal-organic framework nanozymes and integrated smartphone to detection isoniazid, *Sens. Actuators, B*, 2023, **390**, 134024, DOI: 10.1016/j.snb.2023.134024.

54 F. Beygnezhad, K. Dashtian, R. Zare-Dorabei and Z. Zangouei, Biological Ce/Fe-metal organic framework multifunctional nanozyme-based colorimetric sensor array for multi-analyte detection in human sweat, *Sens. Actuators, B*, 2025, **423**, 136769, DOI: 10.1016/j.snb.2024.136769.

55 M. Nejati, M. Kalhori, Z. Zangouei, S. Dastani, K. Dashtian, R. Zare-Dorabei and K. Kerman, Tri-responsive multifunctional metal–organic framework (MuF-MOF) nanozyme-based sensors, *J. Mater. Chem. A*, 2026, **14**, 11145–11202, DOI: 10.1039/D5TA08531D.

56 I. Nath, J. Chakraborty and F. Verpoort, Metal organic frameworks mimicking natural enzymes: a structural and functional analogy, *Chem. Soc. Rev.*, 2016, **45**, 4127–4170, DOI: 10.1039/C6CS00047A.

57 X. Lian, Y. Fang, E. Joseph, Q. Wang, J. Li, S. Banerjee, C. Lollar, X. Wang and H.-C. Zhou, Enzyme–MOF (metal–organic framework) composites, *Chem. Soc. Rev.*, 2017, **46**, 3386–3401, DOI: 10.1039/C7CS00058H.

58 J. Chai, L. Yuan, S. Wang, T. Li, M. Wu, Z. Huang and H. Yin, A series of novel Cu-based MOFs: syntheses, structural diversity, catalytic properties and mimic peroxidase activity for colorimetric detection of H2O2, *New J. Chem.*, 2022, **46**, 12372–12380, DOI: 10.1039/D2NJ01981G.

59 H. Yang, J. Liu, X. Feng, F. Nie and G. Yang, A novel copper-based metal-organic framework as a peroxidase-mimicking enzyme and its glucose chemiluminescence sensing application, *Anal. Bioanal. Chem.*, 2021, **413**, 4407–4416, DOI: 10.1007/s00216-021-03394-5.

60 S. Maity, D. Bain, S. Chakraborty, S. Kolay and A. Patra, Copper Nanocluster (Cu23 NC)-Based Biomimetic System with Peroxidase Activity, *ACS Sustain. Chem. Eng.*, 2020, **8**, 18335–18344, DOI: 10.1021/acssuschemeng.0c07431.

61 A. T. Smith, A. M. LaChance, S. Zeng, B. Liu and L. Sun, Synthesis, properties, and applications of graphene oxide/reduced graphene oxide and their nanocomposites, *Nano Mater. Sci.*, 2019, **1**, 31–47, DOI: 10.1016/j.nanoms.2019.02.004.

62 A. Tripathi and M. P. Styczynski, Copper nanocubes as low-cost enzyme mimics in a sarcosine-sensing reaction cascade, *Analyst*, 2025, **150**, 1248–1260, DOI: 10.1039/D4AN01242A.

63 X. Ruan, D. Liu, X. Niu, Y. Wang, C. D. Simpson, N. Cheng, D. Du and Y. Lin, 2D Graphene Oxide/Fe-MOF Nanozyme Nest with Superior Peroxidase-Like Activity and Its Application for Detection of Woodsmoke Exposure Biomarker, *Anal. Chem.*, 2019, **91**, 13847–13854, DOI: 10.1021/acs.analchem.9b03321.

64 Z. Song, C. Jiang, F. Wang, L. Yu, S. Ye, P. Dramou and H. He, Nanozyme based on graphene oxide modified with Fe3O4, CuO, and cucurbit[6]uril for colorimetric determination of homocysteine, *Microchim. Acta*, 2021, **188**, 207, DOI: 10.1007/s00604-021-04868-0.

65 Decorating Zirconium on Graphene Oxide to Design a Multifunctional Nanozyme for Eco-Friendly Detection of Hydrogen Peroxide.

66 P. Arul, C. Nandhini, S.-T. Huang, C.-H. Huang and K. Shanmugaraj, Design of Zn-MOF/GO-doped CuO as a two-in-one nanozyme signal amplifier for rapid and ultrasensitive smartphone-assisted colorimetric and electrochemical quantification of dual benzenediol environmental hazards, *J. Environ. Chem. Eng.*, 2025, **13**, 119353, DOI: 10.1016/j.jece.2025.119353.

67 K. Sivasankar, K. K. Rani, S.-F. Wang, R. Devasenathipathy and C.-H. Lin, Copper Nanoparticle and Nitrogen Doped Graphite Oxide Based Biosensor for the Sensitive

Determination of Glucose, *Nanomaterials*, 2018, **8**, 1–14, DOI: 10.3390/nano8060429.

68 E. P. Commission, European Pharmacopoeia 7.0 : Buffer Solutions (section 4.1.3.), *European Directorate for the Quality of Medicines*, Council of Europe, Strasbourg, France, 7th edn, 2008, p. 489.

69 H. Cao, Y. Yuan, R. Zhao, W. Shi, J. Jiang, Y. Gao, L. Chen and L. Gao, Deciphering the Catalytic Mechanism of Peroxidase-like Activity of Iron Sulfide Nanozymes, *ACS Appl. Mater. Interfaces*, 2024, **16**, 30958–30966, DOI: 10.1021/acsami.4c06024.

70 X. Li, L. Fu, F. Chen, Y. Lv, S. Zhao and H. Karimi-Maleh, Research on the application of metal-organic framework (MOF)-based nanozymes in colorimetric and electrochemical detection of biomolecules, *Inorg. Chem. Commun.*, 2025, **179**, 114752, DOI: 10.1016/j.inoche.2025.114752.

71 S. Liang, T. Chen, Y. Zhao, Y. Ren, M. Li, D. Lu, J. Wang, Y. Dai and Y. Guo, Revealing the intrinsic peroxidase-like catalytic mechanism of O-doped CoS2 nanoparticles, *Nanoscale*, 2023, **15**, 13666–13674, DOI: 10.1039/D3NR02496B.

72 N. Szpisják-Gulyás, A. N. Al-Tayawi, Z. H. Horváth, Z. László, S. Kertész and C. Hodúr, Methods for experimental design, central composite design and the Box–Behnken design, to optimise operational parameters: A review, *Acta Aliment.*, 2023, **52**, 521–537, DOI: 10.1556/066.2023.00235.

73 A. S. Fayed, M. R. Rezk, H. M. Marzouk and S. S. Abbas, A Capillary Zone Electrophoresis Method with Multiresponse Chemometric Optimization for the Simultaneous Determination of Zofenopril Calcium and Hydrochlorothiazide in Presence of Hydrochlorothiazide Major Impurities, *J. Chromatogr. Sci.*, 2018, **56**, 461–471, DOI: 10.1093/chromsci/bmy014.

74 A. M. Saleh, O. A. Saleh, R. Y. A. Hassan, A. M. Badawey and H. M. Marzouk, A novel quality-by-design assisted HPLC-DAD method for the simultaneous quantification of tryptophan, tryptophol, and voriconazole for early diagnosis and prognosis of fungal infections decoding quorum sensing phenomenon, *J. Chromatogr. B*, 2025, **1257**, 124571, DOI: 10.1016/j.jchromb.2025.124571.

75 J. Ermer, ICH Q2 (R2): validation of analytical procedures, *Method Validation in Pharmaceutical Analysis: a Guide to Best Practice*, 2025, 351–372, DOI: 10.1002/9783527831708.ch13.

76 O. Shekhah, J. Liu, R. A. Fischer and C. Wöll, MOF thin films: existing and future applications, *Chem. Soc. Rev.*, 2011, **40**, 1081–1106, DOI: 10.1039/C0CS00147C.

77 G. G. da Silva, F. L. A. Machado, S. A. Junior and E. Padrón-Hernández, Metal-organic framework: Structure and magnetic properties of [Cu3(BTC)2 (L)x·(CuO)y]n (L=H2O, DMF), *J. Solid State Chem.*, 2017, **253**, 1–5, DOI: 10.1016/j.jssc.2017.05.023.

78 T. Toyao, K. Liang, K. Okada, R. Ricco, M. J. Styles, Y. Tokudome, Y. Horiuchi, A. J. Hill, M. Takahashi, M. Matsuoka and P. Falcaro, Positioning of the HKUST-1 metal–organic framework (Cu3(BTC)2) through conversion from insoluble Cu-based precursors, *Inorg. Chem. Front.*, 2015, **2**, 434–441, DOI: 10.1039/C4QI00215F.

79 A. F. Payam, S. Khalil and S. Chakrabarti, Synthesis and Characterization of MOF-Derived Structures: Recent Advances and Future Perspectives, *Small*, 2024, **20**, 2310348, DOI: 10.1002/smll.202310348.

80 Y.-S. Bae, A. Ö. Yazaydın and R. Q. Snurr, Evaluation of the BET Method for Determining Surface Areas of MOFs and Zeolites that Contain Ultra-Micropores, *Langmuir*, 2010, **26**, 5475–5483, DOI: 10.1021/la100449z.

81 J. Lincke, D. Lässig, J. Moellmer, C. Reichenbach, A. Puls, A. Moeller, R. Gläser, G. Kalies, R. Staudt and H. Krautscheid, A novel copper-based MOF material: Synthesis, characterization and adsorption studies, *Microporous Mesoporous Mater.*, 2011, **142**, 62–69, DOI: 10.1016/j.micromeso.2010.11.017.

82 F. Ambroz, T. J. Macdonald, V. Martis and I. P. Parkin, Evaluation of the BET Theory for the Characterization of Meso and Microporous MOFs, *Small Methods*, 2018, **2**, 1800173, DOI: 10.1002/smtd.201800173.

83 S. Wang, B. Ye, C. An, J. Wang and Q. Li, Synergistic effects between Cu metal–organic framework (Cu-MOF) and carbon nanomaterials for the catalyzation of the thermal decomposition of ammonium perchlorate (AP), *J. Mater. Sci.*, 2019, **54**, 4928–4941, DOI: 10.1007/s10853-018-03219-4.

84 C. Berthomieu and R. Hienerwadel, Fourier transform infrared (FTIR) spectroscopy, *Photosynth. Res.*, 2009, **101**, 157–170, DOI: 10.1007/s11120-009-9439-x.

85 H. Korucu, A. I. Mohamed, A. Yartaşı and M. Uğur, The detailed Characterization of graphene oxide, *Chem. Pap.*, 2023, **77**, 5787–5806, DOI: 10.1007/s11696-023-02897-y.

86 J. Epp, 4 – X-ray diffraction (XRD) techniques for materials characterization, *Materials Characterization Using Nondestructive Evaluation (NDE) Methods*, ed. G. Hübschen, I. Altpeter, R. Tschuncky, and H.-G. Herrmann, Woodhead Publishing, 2016, pp. 81–124, DOI: 10.1016/B978-0-08-100040-3.00004-3.

87 A. H. Shah, Z. U. Abideen, S. Maqsood, F. Rashid, R. Ullah, A. U. Rehman, M. Dildar, M. Ahmad, K. Ullah, M. N. Rafi and F. Teng, Porous Cu-based metal organic framework (Cu-MOF) for highly selective adsorption of organic pollutants, *J. Solid State Chem.*, 2023, **322**, 123935, DOI: 10.1016/j.jssc.2023.123935.

88 A. N. Popova, Crystallographic analysis of graphite by X-Ray diffraction, *Coke Chem.*, 2017, **60**, 361–365, DOI: 10.3103/S1068364X17090058.

89 *ICDD PDF-4+ Database*.

90 T. Liu, B. Fu, J. Chen and K. Li, An electrochemical sarcosine sensor based on biomimetic recognition, *Microchim. Acta*, 2019, **186**, 136, DOI: 10.1007/s00604-019-3240-0.

91 R. Etzioni, S. Falcon, P. H. Gann, C. L. Kooperberg, D. F. Penson and M. J. Stampfer, Prostate-specific antigen and free prostate-specific antigen in the early detection of prostate cancer: do combination tests improve detection?, *Cancer Epidemiol., Biomarkers Prev.*, 2004, **13**, 1640–1645, DOI: 10.1158/1055-9965.1640.13.10.

92 N. Cernei, Z. Heger, J. Gumulec, O. Zitka, M. Masarik, P. Babula, T. Eckschlager, M. Stiborova, R. Kizek and V. Adam, Sarcosine as a Potential Prostate Cancer Biomarker—A Review, *Int. J. Mol. Sci.*, 2013, **14**, 13893–13908, DOI: 10.3390/ijms140713893.

93 S. Erdemir and S. Malkondu, On-site and low-cost detection of cyanide by simple colorimetric and fluorogenic sensors: Smartphone and test strip applications, *Talanta*, 2020, **207**, 120278, DOI: 10.1016/j.talanta.2019.120278.

94 P. Yadav, L. Yadav, H. Laddha, M. Agarwal and R. Gupta, Upsurgence of smartphone as an economical, portable, and consumer-friendly analytical device/interface platform for digital sensing of hazardous environmental ions, *Trends Environ. Anal. Chem.*, 2022, **36**, e00177, DOI: 10.1016/j.teac.2022.e00177.